Algorithm based comparison between the integral method and harmonic analysis of the timing jitter of diode-based and solid-state pulsed laser sources

Optics Communications 341 (2015) 7–14

Contents lists available at ScienceDirect

Optics Communications

journal homepage: www.elsevier.com/locate/optcom

Algorithm based comparison between the integral method and harmonic analysis of the timing jitter of diode-based and solid-state pulsed laser sources

N.K. Metzger [a,*], C.-R. Su [b], T.J. Edwards [b], C.T.A. Brown [b]

[a] SUPA School of Engineering and Physical Sciences, Photonics & Quantum Sciences, Heriot Watt University, Edinburgh EH14 4AS, UK
[b] SUPA School of Physics and Astronomy, University of St Andrews, North Haugh, St Andrews, Fife KY16 9SS, UK

ARTICLE INFO

Article history:
Received 21 August 2014
Received in revised form
25 November 2014
Accepted 27 November 2014
Available online 3 December 2014

Keywords:
Phase noise
Timing jitter
Semiconductor lasers
Mode-locked lasers
Pulsed laser noise
Pulse train
Laser stabilization

ABSTRACT

A comparison between two methods of timing jitter calculation is presented. The integral method utilizes spectral area of the single side-band (SSB) phase noise spectrum to calculate root mean square (rms) timing jitter. In contrast the harmonic analysis exploits the uppermost noise power in high harmonics to retrieve timing fluctuation. The results obtained show that a consistent timing jitter of 1.2 ps is found by the integral method and harmonic analysis in gain-switched laser diodes with an external cavity scheme. A comparison of the two approaches in noise measurement of a diode-pumped Yb:KY$(WO_4)_2$ passively mode-locked laser is also shown in which both techniques give 2 ps rms timing jitter.

1. Introduction

Actively and passively mode-locked lasers are ideal candidates for the generation of coherent, stable and highly periodical pulse trains. They have been the subject of intense investigation as they can be used in many applications, including high-speed optical communications, all-optical signal-processing, optical sampling and clock distribution [1]. Among these applications, some require not only high peak power and short pulse operation, but also the smallest possible timing jitter, as the fluctuation of the time interval between pulses degrades the quality of the expected system performance.

A broad bandwidth oscillator can detect timing fluctuations by monitoring the beat frequency between a modulated signal and low-jitter electrical trigger signal [2]. This enables one to easily obtain the exact timing fluctuation of an unknown optical source. Although this is an accurate method to calculate timing jitter, the equipment requirement of a broad bandwidth and a trigger-dependent source limits the practicality of such spectral measurements. These drawbacks can be overcome with the combination of a fast photodetector and an electronic spectrum analyzer. The available bandwidth of the spectrum analyzer not only facilitates measurements, but also provides important insight into sources of both correlated and uncorrelated timing jitter [2,3].

By considering the noise sideband of the power spectrum, phase noise can be distinguished from amplitude fluctuation. Whilst phase noise rises quadratically with harmonic order, amplitude fluctuation remains order independent across the full frequency spectrum [2]. Both of these effects contribute to pedestals or broad noise sidebands that prevent a clean RF signal. The single side-band (SSB) phase noise, which is identified by the carrier per resolution bandwidth, reveals information about the timing jitter. Following von der Linde's work [2], the rms timing fluctuation at a given carrier frequency f_R can be obtained from a spectral integration of noise if the rms amplitude noise remains small.

When using this method the integration boundaries need to be chosen carefully [4–12] to obtain high measurement accuracy. To solve this problem, an approach using a simplified theoretical model has been developed [2]. The harmonic approach adjusts the integration by utilizing the uppermost noise power to identify the timing jitter in higher harmonic orders. This has been verified as a valid solution [9,10], yet it remains relatively little used compared to the integration method discussed above. This is because the accuracy of harmonic analysis is greatly restricted by the highest

* Corresponding author. Fax: +44 131 451 3473.
E-mail address: k.metzger@hw.ac.uk (N.K. Metzger).

http://dx.doi.org/10.1016/j.optcom.2014.11.088
0030-4018/

harmonic order obtained; the higher the harmonic order, the more precise the timing jitter.

To date, a thorough comparison of both methods has yet to be conducted, despite Ng et al. [11] and Yoshida [12] confirming the consistent outcome of these two approaches in their own system. This publication presents two studies of the rms timing jitter calculated by the integral method as well as the harmonic analysis approach in gain-switched semiconductor laser diodes. The calculated timing jitter of 1.1 ps and 1.25 ps obtained by harmonic analysis and integral method respectively in this work, proved comparable to the 1.5 ps jitter in a Fabry–Perot gain-switched semiconductor laser diode with optical feedback [13,14]. These two algorithms were then applied to an Yb:KYW passive mode-locked lasers and yielded a free-running jitter time of 2.05 ps and 1.95 ps respectively. A similar agreement of results was obtained with an Yb:Eb:glass ultrafast laser [15].

The outcomes of this study validates the consistent measurement of timing jitter by both the harmonic analysis and integral method when tested theoretically and experimentally in mode-locked and gain-switched lasers.

2. Background to jitter measurements and algorithm development

The well-developed theory by von der Linde has been used to calculate rms timing jitter in spectral measurements [2]. This work analyzed the noise behavior in the power spectrum and found that noise varies with increasing harmonic orders. While amplitude noise remains a frequency-independent trend, phase noise increases quadratically and further becomes the main source of noise for high harmonics in RFSA. Phase noise is thus observed to have the largest contribution with respect to rms timing jitter. To compute timing jitter, there are two approaches advocated.

The first approach, the integral method, uses the integration of the entire SSB phase noise to calculate the rms timing jitter. This approach assumes that the amplitude fluctuation is negligible in affecting the power spectrum. The second, harmonic analysis, is a simplified version of the integral method. This utilizes the whole power spectrum and then retrieves the uppermost noise power and full width at half maximum (FWHM) noise bandwidths in high harmonic orders for the calculation of rms timing jitter. Both methods have been validated to be correct theoretically and experimentally [3,9,11,12,16,17].

In order to compare rms timing jitter efficiently, these two methods were implemented in Matlab. The content of these programs for harmonic analysis and the integral method will be discussed in the following sections.

2.1. Algorithm for harmonic analysis

Before calculating rms timing jitter, harmonic analysis requires information from the RFSA trace. A fluctuation-free pulse train is seen to have a delta RF linewidth. However, once the pulse encounters phase noise, an undefined phase relation between each pulse will result in the broadened linewidth RFSA trace shown in Fig. 1. After the red crosses (P_B), the power spectrum encounters noise interruption.

In Fig. 1, P_A denotes the peak of the RFSA trace. P_B and P_C represent the power of the maximum noise level and the averaged noise floor respectively.

The rms timing jitter can be estimated [2] with Eq. (1), given prior knowledge of parameters P_A, P_B, P_C, Δf_{res} resolution bandwidth (RBW), Δf_J (the FWHM of noise bands), round trip time T, and the harmonic order n of the measured RFSA data in Eq. (1).

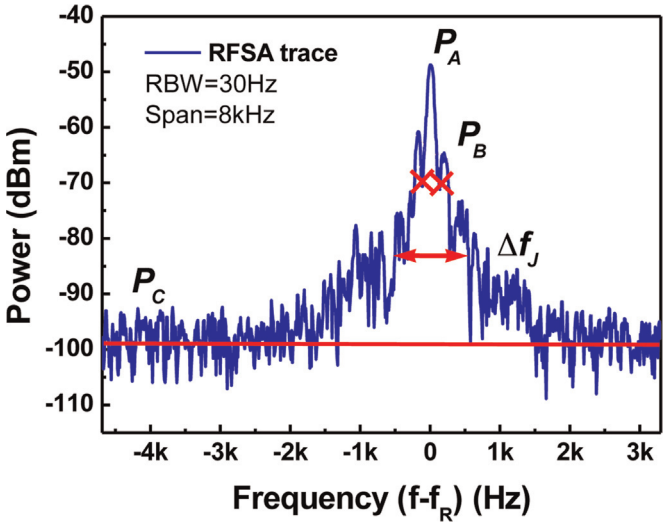

Fig. 1. The RFSA trace obtained with Matlab (RBW = 30 Hz). The RFSA trace shows large noise interference until the trace reaches the noise floor. P_A marks the peak of the RFSA trace. P_B represents the power of the maximum noise level and P_C the averaged noise floor while Δf_J is the FWHM level between P_c and P_B. (For interpretation of the references to color in this figure, the reader is referred to the web version of this article.)

$$\Delta t = T(2\pi n)\left[\left(\frac{P_B}{P_A}\right)_n \frac{\Delta f_J}{\Delta f_{res}}\right]^{1/2} \quad (1)$$

where Δt symbolizes the rms timing jitter. P_B the uppermost noise level (red crosses in Fig. 1) is determined automatically as illustrated in Fig. 2.

Initially, the unprocessed RFSA data is convoluted with a moving average filter generated by the analysis program to remove spurious aliasing ripples. From this filtered curve Fig. 2(a), the algorithm is able to extract its slope. The slope of the raw RFSA data and its filtered curve slope are both depicted in Fig. 2(b) by the blue curve and red dotted curve, respectively. Looking back at the original data in Fig. 2(a), it can be seen that the uppermost phase noise has a local minima, shown in the expanded (c). Furthermore, the local maximum or minimum points in Fig. 2(c) will have a value of approximately zero at the same frequencies in (d). It is not surprising that the extreme values usually result from the transition in slope. Therefore, to find the uppermost noise, the program can rely on the transition point of the slope. In other words, values where there are zero crossings Fig. 2(d) correspond to the extreme values of (c).

Similarly P_A and P_C can both be obtained from a standard maximum and minimum search function where P_C was taken as the average noise floor. The points (f_{J1} and f_{J2}) both have powers of $(P_B+P_C)/2$ in the power spectrum, where the corresponding frequency distance between the two points determines the FWHM of the noise bandwidths $\Delta f_J = f_{J1} - f_{J2}$. Roundtrip time T, harmonic order n, and RBW can be retrieved from the RFSA trace. This method assumes no correlations between the intensity and phase noise of the pulses [2]. When timing-jitter fluctuations between pulses are uncorrelated in time a Lorentzian shaped RFSA trace is obtained. Correlations between timing fluctuations tend to produce traces that are Gaussian in shape [6]. In the first case the accuracy of the prediction of the jitter will suffer however the algorithm will still give a fast qualitative prediction as shown in experimental section.

2.2. Amplitude fluctuations

Although amplitude noise remains a small value for most frequencies, it nevertheless influences the power spectrum regarding

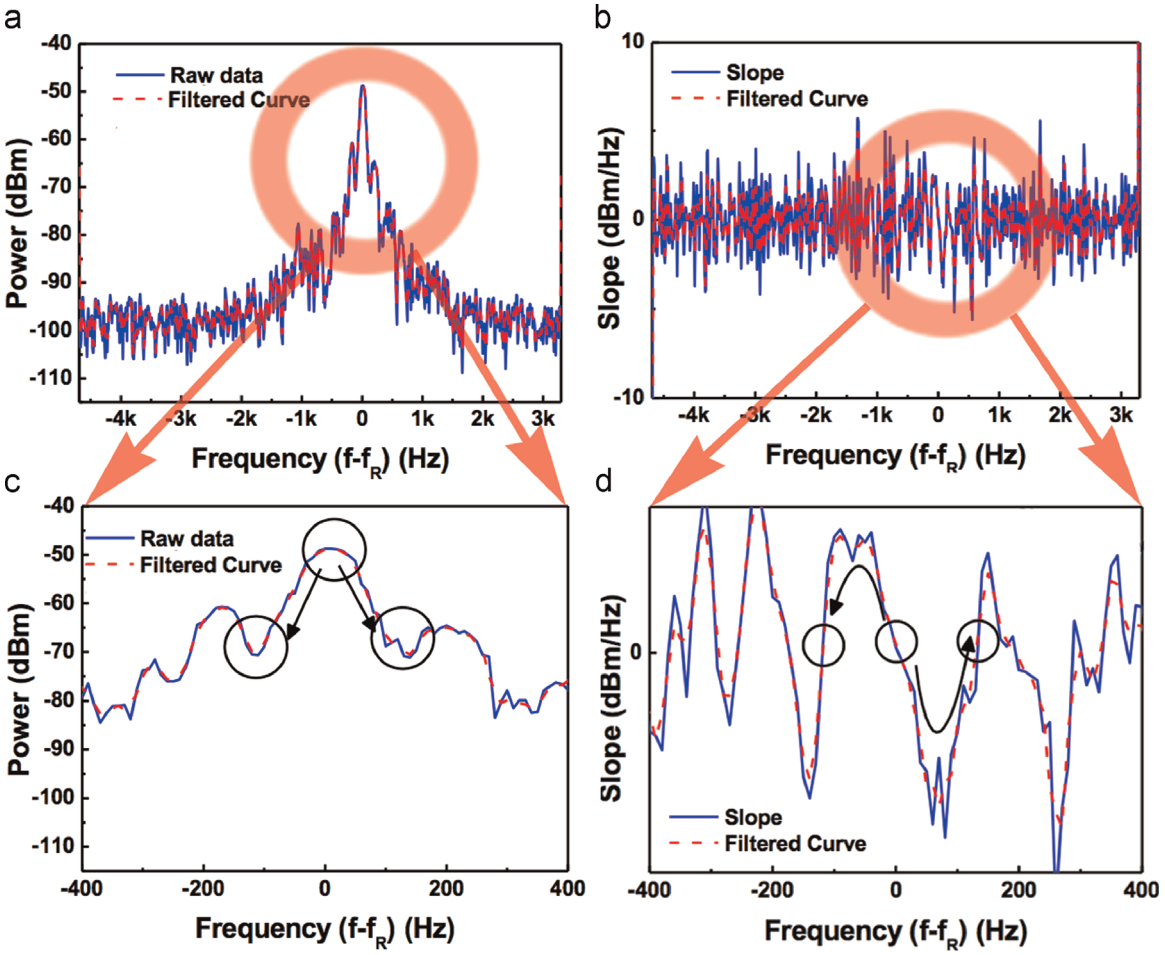

Fig. 2. The illustration of harmonic analysis (a) the raw RFSA trace (blue curve) and the filtered curve (red dashed line) with a RBW of 30 Hz. (b) The slope of the RFSA data (blue curve) and its filtered curve (red dashed). (c) The 800 Hz span zoomed-in version of (a). The black arrows indicate the direction of the search of the algorithm. (d) 800 Hz span zoomed-in version of (b). The black arrows indicate the direction of the search of the algorithm. (For interpretation of the references to color in this figure legend, the reader is referred to the web version of this article.)

lower harmonic orders [2]. Zero-order noise has especially been found to be influenced most by energy instability. This behavior is described below in Eq. (2)

$$\Delta E/E = \left[(P_B/P_A)_0 \Delta f_A/\Delta f_{res}\right]^{1/2} \tag{2}$$

where $\Delta E/E$ is the amplitude fluctuation, P_B is the maximum of noise level, P_A is the peak power, Δf_A is the FWHM of the zero order noise bands and Δf_{res} is the resolution bandwidth. It can be seen that the equation is very similar to Eq. (1), except that the harmonic order is zero. Therefore the Matlab based harmonic analysis algorithm can be applied to evaluate energy fluctuation when the carrier frequency is set at DC.

2.3. Integral method

In a second approach the integral method was used to automatically determine the noise level. When using the integral method to calculate the timing jitter, it is necessary to obtain the SSB phase noise spectrum. The SSB phase noise spectrum, $L(f)$, is defined as the ratio of noise in a 1 Hz resolution bandwidth at a specified frequency offset f to the oscillator signal amplitude at carrier frequency f_n. Eq. (3) illustrates this concept [16]

$$L(f) = \log_{10}\left[\frac{P_F(f)}{P_A \Delta f_{res}}\right] \tag{3}$$

where $P_F(f)$ is the SSB noise spectral density, P_A is the carrier power, and Δf_{res} resolution bandwidth (RBW). For higher harmonic orders, $P_F(f)$ will be dominated by the SSB phase noise spectral density $P_J(f)$ [16]. Where $L(f)$ is obtained from the RFSA trace in units of dBc/Hz. The spectral area of the power spectrum can be directly related to the timing fluctuation by Eq. (4)

$$t_j = \frac{1}{2\pi f_n}\sqrt{\int_{f_n+f_{min}}^{f_n+f_{max}} L(f)df + \int_{f_n-f_{max}}^{f_n-f_{min}} L(f)df} \tag{4}$$

where f_n is the carrier frequency at harmonic order n, $L(f)$ is the SSB phase noise spectrum, and t_j is the rms timing jitter. In the equation, f_{max} and f_{min} are the upper and lower boundaries for integration.

Because of its simple numerical formula, the integral method is most commonly used for calculating timing jitter. An algorithm for the integration method can be implemented by simply performing integration via the trapezoidal method.

Despite being a convenient way to determine timing jitter, care has to be taken when defining the integration boundaries f_{max} (upper boundary) and f_{min} (lower boundary) [2].

In this work the lower integration boundary (f_{min}) was determined through the aid of the harmonic algorithm. Fig. 3 (a) shows the 14th order SSB phase noise $L(f)$ in the RF spectrum. The red cross represents P_B the power of the maximum noise level as used for the harmonic analysis. In Fig. 3(b) the normalized $L(f)$ from harmonic orders 1–14 is shown.

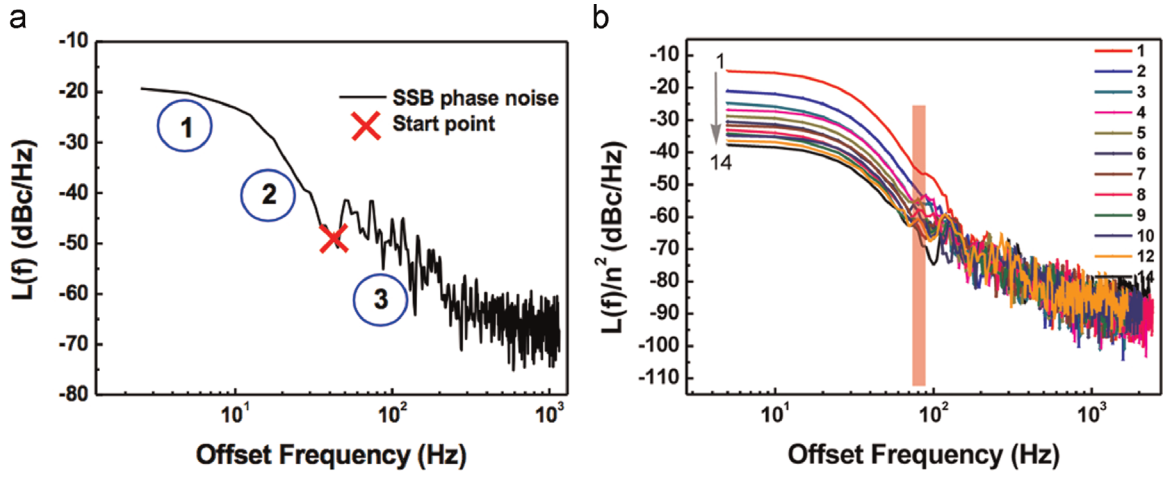

Fig. 3. (a) The SSB phase noise spectrum (acquired with a RBW of 80 Hz) of harmonic order $n=14$ with three different slopes; (b) the normalized SSB phase noise depicted with varied harmonic orders from $n=1$ to 14. With f_{min} being within offset frequencies 80–90 Hz as highlighted in red. (For interpretation of the references to color in this figure legend, the reader is referred to the web version of this article.)

The curve in Fig. 3(a) can be divided into three regions. The first section from 5 Hz to 20 Hz displays a white plateau as marked 1. The second section ranging from 20 Hz to 40 Hz shows accelerated degradation. Beyond 40 Hz, the third section shows a decaying trend of 20 dBc/Hz per decade due to phase noise marked as 3. Fig. 3(b) demonstrates the respective normalized SSB phase noise with varying order n. The lower integration boundary (f_{min}) are within offset frequencies 80–90 Hz as highlighted in Fig. 3(b). After this the normalized SSB phase noise scales and aligns each other accordingly to their respective order number n from 1 to 14.

These lower boundaries were determined by the harmonic analysis algorithm as indicated by the red cross in Fig. 3(a). According to the algorithm's search result, the pure signal and phase noise can be separated, thus demonstrating the viability of the Matlab algorithm to identify phase noise.

The upper integration boundary f_{max} has an approximate limit. Typically f_{max} is half the span [11,18] or the point where phase noise hits the thermal noise floor [4,19]. In the analysis presented here the upper integration boundary was selected to be at the intercept where the noise floor meets the phase noise, to be analogous with the harmonic analysis and the slope is not at 20 dBc/Hz per decade. In the following example this is illustrated: the integral algorithm employed $f_{min}=0.5$ kHz, found by the harmonic algorithm as a lower integration boundary and the upper integration boundary was $f_{max}=10$ kHz as the intercept with the noise floor. The noise floor therefore determines the upper boundary and hence these fluctuations are not accounted for in the integral. This aids to reduce the contribution of amplitude fluctuations to the analysis under the assumption that the timing jitter within the integral boarders is correlated and amplitude fluctuations are small and do not affect the phase [2]. Fig. 4 demonstrates the resulting integration boundaries.

In the analysis shown in Fig. 4, a jitter of 2.85 ps was obtained compared to a jitter value of 2.59 ps obtained for the same dataset using the Harmonic analysis. To check the robustness of our approach several measurements were conducted from which a precision of $\pm 6\%$ was estimated.

Integration of the entire area from f_{min} to half of the measurement span as used in Refs. [18,20] results in an increase of the calculated jitter by about 15%, which is similar to [21]. Thus it can be seen that the spectral area related to phase noise is affected by the correct choice of f_{max} outside the thermal noise floor. The average noise floor (red line in Fig. 4(a)) was found to be -96.42 dBm whereas f_{max} (red circle in Fig. 4(a)) was determined

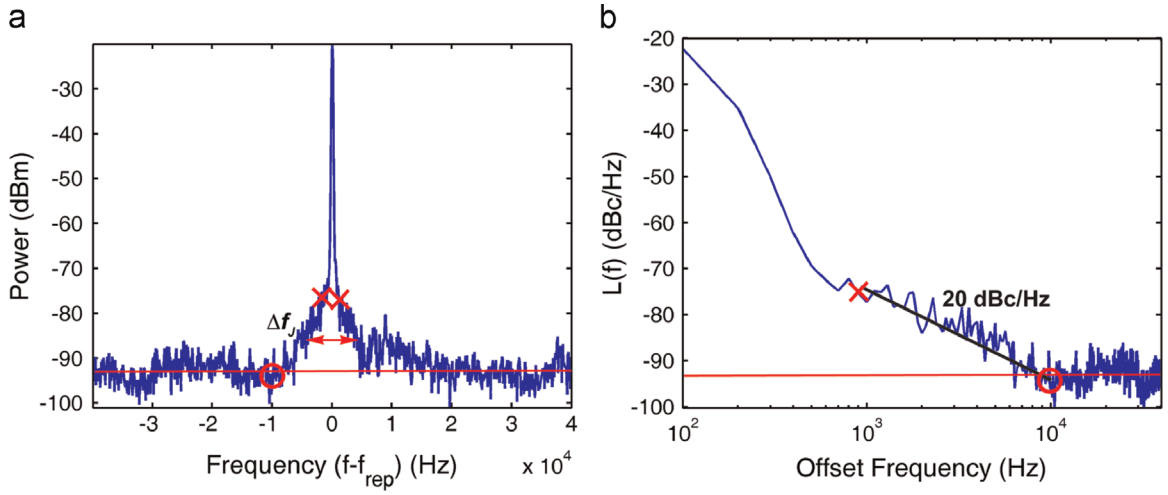

Fig. 4. (a) Harmonic analysis: The RFSA trace (with a RBW of 100 Hz) shows P_B (red crosses) and P_C the average noise floor as a red line as determined by the harmonic algorithm. Addtionally the Δf_J (the FWHM of the noise band) is indicated with the double arrows. The red circles are used as f_{max} by the integral analysis of the left hand SSB. (b) Integral analysis: f_{min} (red cross) is determined by the harmonic analysis. The red circle indicates f_{max} where the noise band intercepts the noise floor. The characteristic 20 dBc/Hz slope is observed between f_{min} and f_{max}. (For interpretation of the references to color in this figure legend, the reader is referred to the web version of this article.)

to −93.45 dBm by the integral analysis. Both values are reasonably close to each other and give confidence in the presented approach to determine the integration boundary. In the following work, f_{min} was set to be equal to that used in the harmonic analysis to enable the comparison between the two approaches.

With these algorithms, we are now well placed to analyze different laser systems and compare their jitter values.

3. Application to picosecond pulses from a gain-switched external cavity diode laser

With the developed algorithm, we assessed the performance of a commercial GaAs tapered diode lasers from m2k-laser (TAL-1060-2000). The laser has a reflectivity 1% at the output facet and anti-reflection coating of 0.01% at the rear facet and was arranged in an external cavity geometry [22,23] as depicted in Fig. 5(a). The laser was operated with a DC offset bias and a supplementary RF-modulated injection current from a signal generator. An electronic amplifier was incorporated to provide an RF power of 35 dBm. The output optical pulses centered at 1060 nm were detected using a fast InGaAs photodiode, which had a time response full-width at half-maximum (FWHM) of 12.5 ps. Care has to be taken not to oversaturate the sensitive detector as permanent damage might occur. For the experiments conducted here an average power of 0.5–0.6 mW was incident on the detector element. This was below the maximum value of 1 mW quoted by the manufacturer for save operation. By blocking the beam into the detector input it was ensured that the acquired RFSA trace was above the detector and RF analyzer noise floor before each measurement. The pulse train was captured using a 22 GHz Radio Frequency Signal Analyzer that was computer interfaced.

The maximum output power is found to be 115 mW when operated at an injection current of 200 mA. The cavity length is chosen to be 23.2 cm give a pulse repetition frequency of 651.1 MHz. The best pulse quality requires a stable signal without any noise induced by self-pulsation. The RFSA trace is found to be Lorentzian shape when the DC current is maintained at 42 mA, and the RF frequency is set at 640.67 MHz. These results correspond to those obtained in similar gain-switched schemes [13]. With the parameters chosen above, the RFSA trace can be seen up to the 7th harmonic order in the system.

The jitter algorithm was applied to all seven harmonic orders. The harmonic approach and integral method in the RF spectrum are depicted in Fig. 6(a) and (b), respectively.

In Fig. 6(a), the harmonic approach establishes the red starred points as the uppermost powers used to calculate timing jitter. From Fig. 6(b), the spectral area is calculated via integration from $f_{min}=0.9$ kHz to $f_{max}=10$ kHz and is further converted to timing jitter by the integral method. Increasing of the integration border to the full acquisition span $f_{max}=40$ kHz results in an increase of the timing jitter by 13% approximately 3% relative to the increased integration bandwidth indicating that the major contribution to the jitter is in the lower frequency components. Relaxation oscillations for modulated lasers can contribute to the timing jitter but are estimated to be higher than the jitter frequency range of approximately 1–10 kHz considered here. Fig. 7(a) shows that the total phase noise determined by the harmonic and integral method is consistent. The two results both follow the linear tendency of $\phi(n)/\phi(1)=n$ from orders 1 to 7. Consequently, a frequency-independent jitter is obtained from the two algorithms in Fig. 7(b).

From Fig. 7(b), the average jitter [5] is determined to 1.2 ± 0.2 ps and 1.2 ± 0.2 ps for the harmonic and integral method respectively. This corresponds well to the value (1.5 ps) obtained in [13] where the single contact Fabry–Perot gain-switched semiconductor laser diode is operated at twice the DC threshold current with an external cavity scheme. The reduced jitter, which differs from the typical value of the gain-switched edge emitting laser diode (>1.5 ps experimentally and >3.5 ps theoretically [24]), is due to optical feedback, which has been verified to reduce timing jitter greatly [25]. This is because the high coherence of reflected photons suppresses the spontaneous emission of laser diodes [24]. In summary, both the harmonic approach and the integral method give consistent and accurate calculations of timing jitter for this laser system.

4. Application to femtosecond pulses from an mode-locked Yb:KYW laser

We next applied the algorithm to passively mode-locked pulses from a solid state laser. The pulse source used was a diode-pumped Yb:KYW laser similar to the systems developed in [26,27]. The laser was passively mode-locked using a semiconductor saturable absorber mirror and produced of 138 fs duration in the

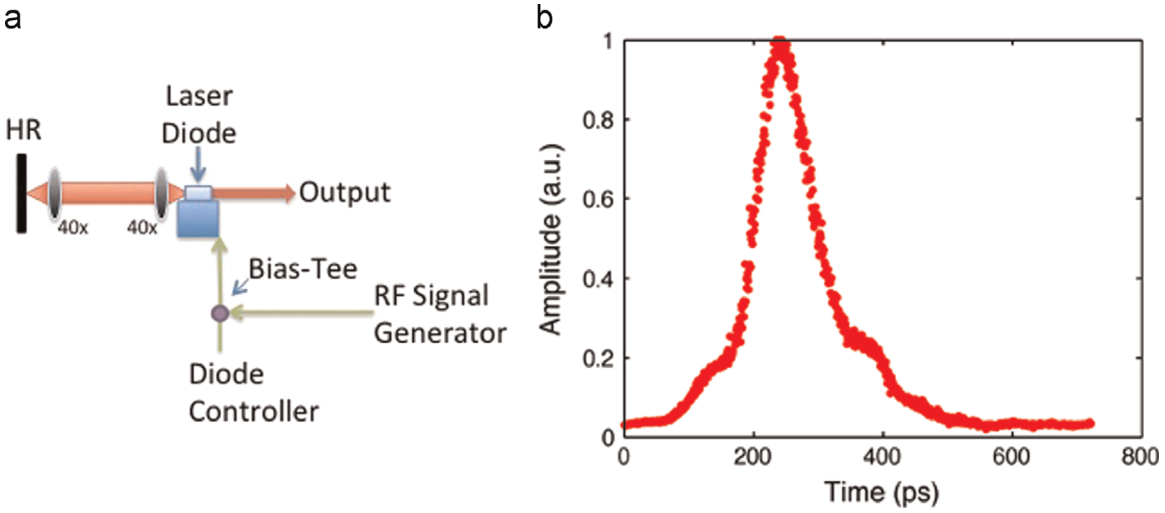

Fig. 5. (a) Layout of the gain-switched laser diode. The external cavity is formed between a HR high reflected mirror and the diode facet. Two 40 × microscope objectives are used to collimate the beam and focus it into the laser diode. A laser diode driver that provided the DC offset in combination with a signal generator via a bias-tee operated the diode. (b) Example pulse obtained from the gain-switched laser diode with pulse duration of about 80 ps at a repetition rate of 0.64 GHz (~23 cm external cavity length).

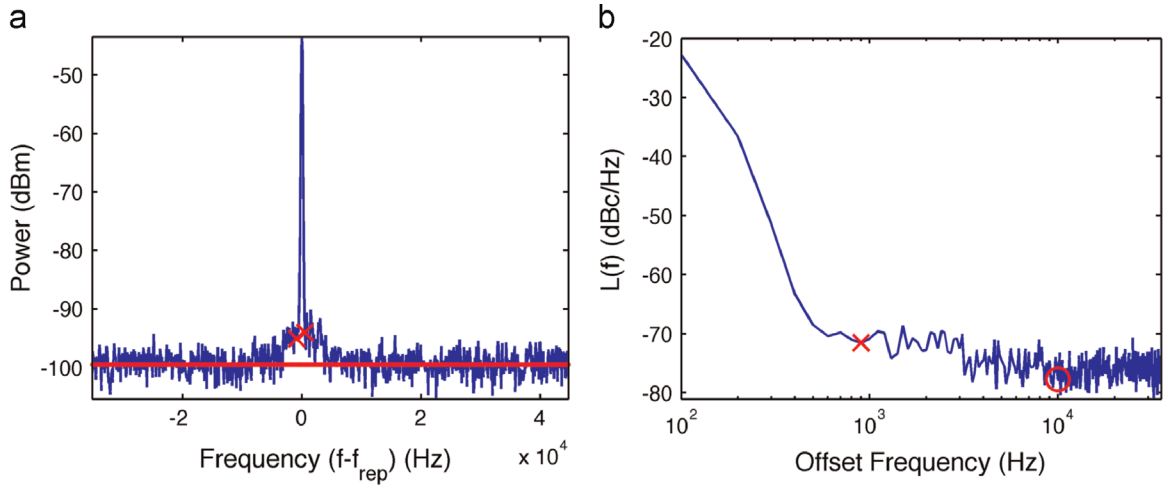

Fig. 6. (a) The RFSA trace of the 7th order in gain-switched laser diode with a RBW of 100 Hz and span of 80 kHz (b) the SSB phase noise spectrum of 7th order with the lower integration $f_{max}=10$ kHz (circle) and the upper boundary $f_{min}=900$ Hz (cross). (For interpretation of the references to color in this figure, the reader is referred to the web version of this article.)

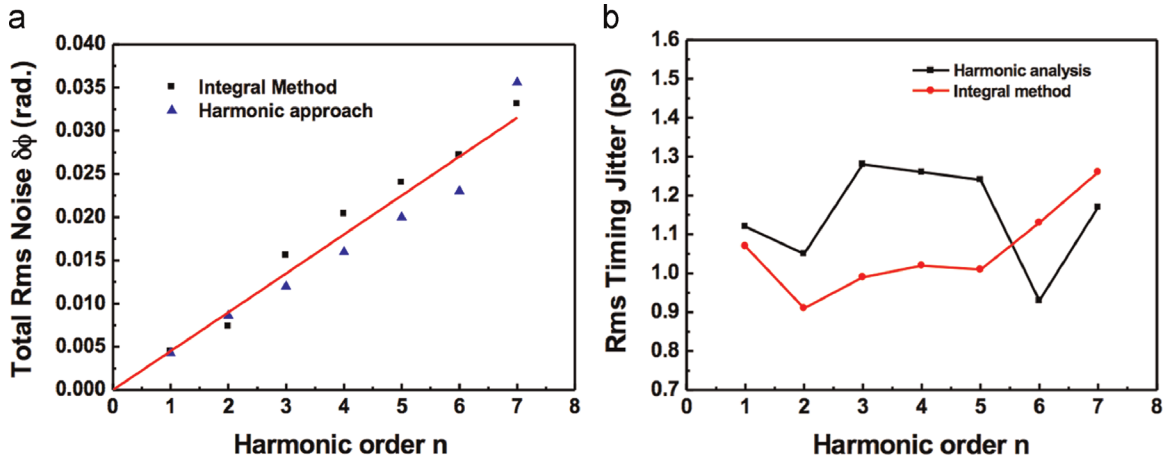

Fig. 7. (a) The rms phase fluctuation determined by the harmonic and integral method and plotted with the theoretical prediction line. (b) The measurement of timing jitter by the two algorithms.

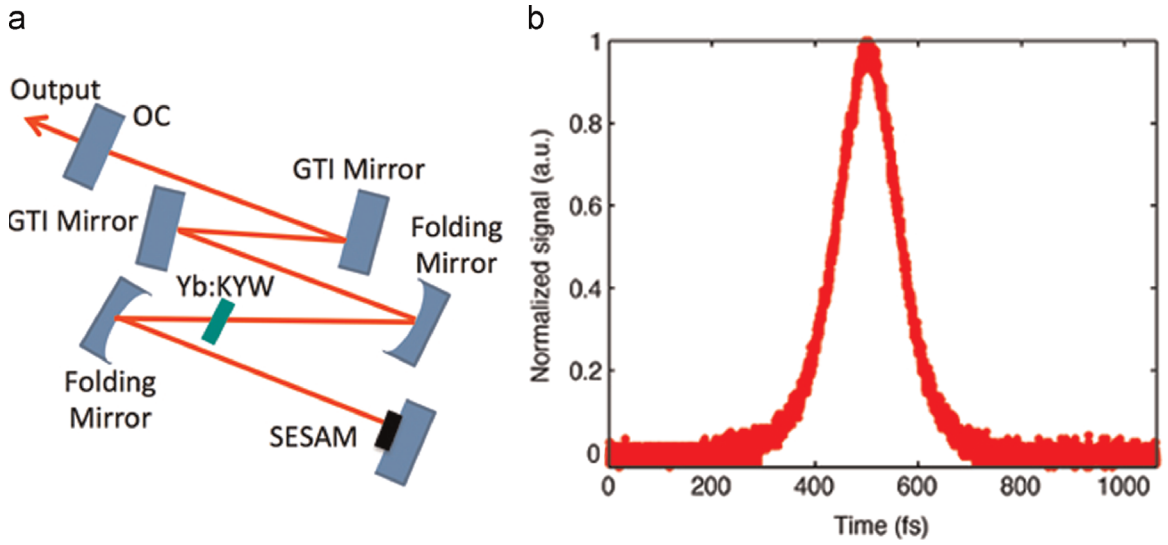

Fig. 8. (a) A schematic of the asymmetric z-fold Yb:KYW cavity. The folding mirrors are spherically curved with radii of curvature of 75 mm. SESAM is a semiconductor saturable absorber mirror ($A=2\%$ and $\Delta R=1.2\%$), while OC is a 3.2% output coupler. Both GTI mirrors provide a single pass dispersion of -910 fs^2. (b) A representative autocorrelation trace of the pulses obtained from the mode-locked Yb:KYW laser with a pulse duration of 138 fs.

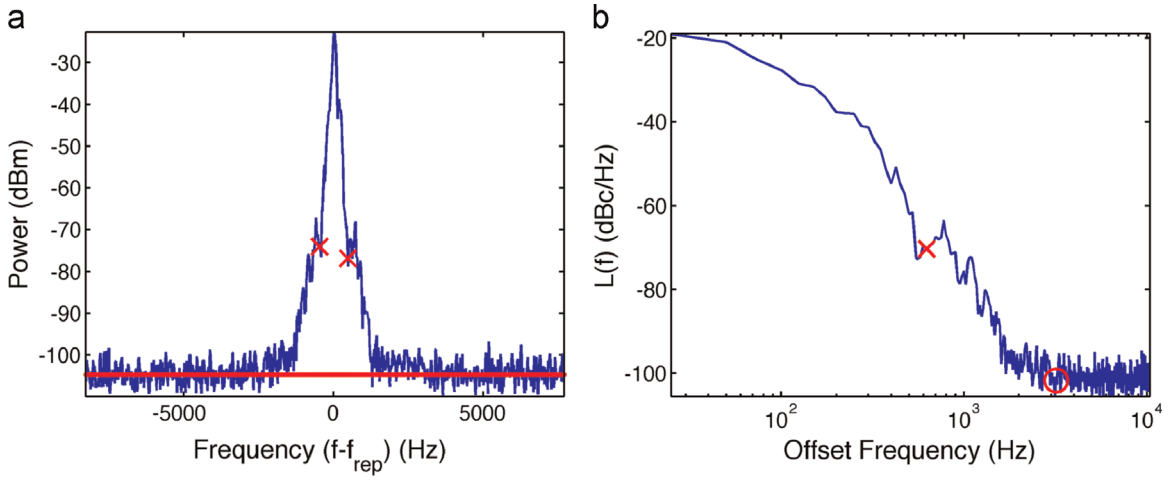

Fig. 9. (a) The RFSA trace for the 7th order with a RBW of 80 Hz, and (b) its SSB phase noise with the lower integration f_{max}=3.2 kHz (circle) and the upper boundary f_{min} =625 Hz (cross).

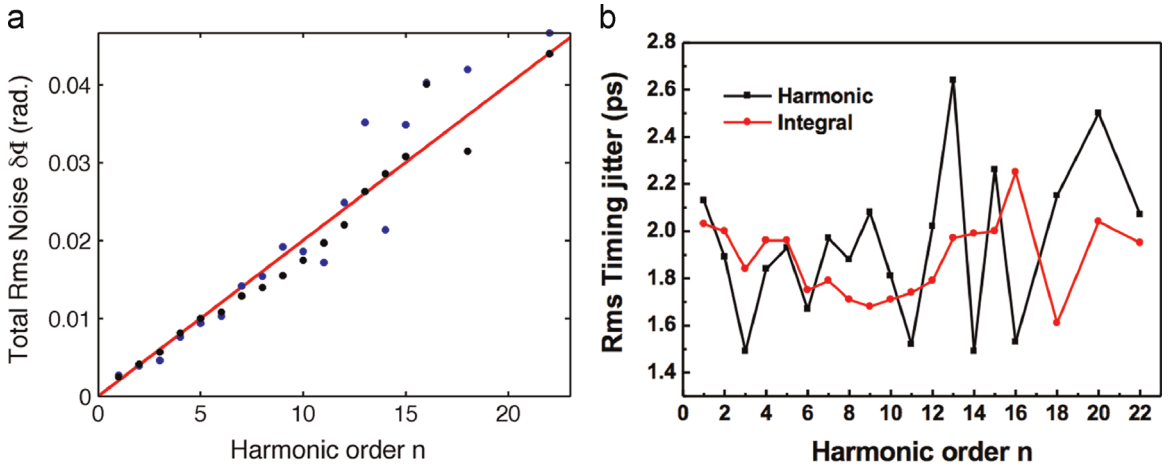

Fig. 10. The timing jitter measurements of a Yb:KYW mode-locked laser (a) the total phase noise fluctuation and (b) the timing jitter of different harmonic orders calculated by the two algorithms.

1035–1040 nm wavelength range with a pulse repetition frequency of 161 MHz at an average output power of 80 mW. The corresponding spectral width for the pulses was 8.5 nm, which implied a time-bandwidth product of 0.33.

The schematic and a measured intensity autocorrelation trace of the mode-locked Yb:KYW laser are shown in Fig. 8.

The output beam is coupled into the same measurement setup as in the previous section via an optical isolator to prevent feedback. The highest harmonic order is found to be 22. In harmonic orders higher than 22, the phase noise interferes with the RFSA trace so strongly that the timing jitter cannot be distinguished.

A high RBW of 80 Hz and span of 20 kHz is chosen to prevent amplitude fluctuation from entering low harmonics. In Fig. 9 the RFSA trace and the resulting SSB trace for the 7th order are shown.

In Fig. 9(b), the noise band has a gradually descending slope in the SSB phase noise spectrum and is found that the noise skirt hits the noise floor at an offset frequency of approximately 3 kHz. Hence, f_{max}=3.1 kHz is selected as a suitable upper boundary and f_{min}=625 Hz is selected as the lower boundary.

Fig. 10(a) shows the evaluation of timing jitter when the amplitude noise is taken to be negligible. Fig. 10(b) illustrates the total rms phase noise with varied harmonic orders.

In Fig. 10(a), the linear trend also obeys the predicted theoretical model detailed previously. In Fig. 10(b), the consistency of harmonic approach and integral method is demonstrated up to the 12th harmonic order. In higher harmonic orders, the phase noise interferes with the RFSA trace more strongly so that the timing jitter cannot be distinguished accurately and the results start to fluctuate. The algorithms determine an average timing jitter [5] of 2.0 ± 0.6 ps and 1.9 ± 0.3 ps for the harmonic and integral method respectively for the different orders. This is a comparable value to the 2.5 ps obtained in a similar soliton mode-locked system [15]. Timing phase noise scales inversely with the intracavity pulse energy and linearly with the square of pulse duration [28]. The discrepancy of 0.5 ps can be explained from the interaction between the lower pulse energy (0.5 nJ) and shorter pulse duration (138 fs) compared to the pulse energy (1.03 nJ) and pulse duration (255 fs) obtained in [15]. In conclusion, harmonic and integral method found an average timing jitter of approximately 2 ps, a value that is much larger than that obtained in active mode-locked systems [14]. To diminish the free-running timing jitter to a femtosecond jitter regime, feedback timing stabilization such as a phase-locked loop (PLL) system can be employed in the same mode-locked system scheme [29].

5. Conclusion

This publication presented the first direct comparison between the harmonic analysis and the integral method of characterizing

timing jitter. The study of both approaches used the theoretical framework developed by von der Linde [2] that has been widely used in RF measurement, and investigated using an automated Matlab program [30]. The algorithm results show that both the harmonic approach and the integral method correspond to the theory appropriately and are reliable in characterizing rms timing jitter. Noise estimation in gain-switched laser diode and Yb:KYW passive mode-locked solid state laser are used to thoroughly compare the two methods.

The applied method relies on direct detection of the pulse train and therefore the dynamic range of the detector limits phase noise measurement of the RF harmonic. These limitations are overcome by employing the optical cross-correlation method [31]. In contrast to the approach applied in this publication it is an all-optical timing jitter characterization method that enables extremely high timing resolution. The optical cross-correlation method has recently been employed for ultralow timing jitter measurement [32] in solid state lasers and also shows good agreement with the integral method when applied to mode-locked laser diodes [33].

Nevertheless the outcomes not only demonstrate a consistent relationship between the two methods but also prove their accuracy in evaluating rms timing jitter, as the values have been confirmed experimentally and theoretically in the same system setup.

Acknowledgments

This work was supported by the European Metrological Research Programme EMRP under IND 14. The EMRP is jointly funded by the EMRP participating countries within EURAMET and the European Union. N.K. Metzger acknowledges support from the EPSRC Centre for Innovative Manufacturing in Laser-based Production Processes, funded through EPSRC grant EP/K030884/1.

References

[1] E.A. Avrutin, J.H. Marsh, E.L. Portnoi, Monolithic and multi-GigaHertz mode-locked semiconductor lasers: constructions, experiments, models and applications, IEEE Proc.—Optoelectron. 147 (2000) 251–278.
[2] D. von der Linde, Characterization of the noise in continuously operating mode-locked lasers, Appl. Phys. B 39 (1986) 201–217.
[3] D.A. Leep, D.A. Holm, Spectral measurement of timing jitter in gain-switched semiconductor lasers, Appl. Phys. Lett. 60 (1992) 2451–2453.
[4] J.P. Tourrenc, A. Akrout, K. Merghem, A. Martinez, F. Lelarge, A. Shen, G. H. Duan, A. Ramdane, Experimental investigation of the timing jitter in self-pulsating quantum-dash lasers operating at 1.55 μm, Opt. Exp. 16 (2008) 17706–17713.
[5] C.Y. Lin, F. Grillot, Y. Li, R. Raghunathan, L.F. Lester, Microwave characterization and stabilization of timing jitter in a quantum-dot passively mode-locked laser via external optical feedback, IEEE J. Sel. Top. Quantum Electron. 17 (2011) 1311–1317.
[6] D. Eliyahu, R.A. Salvatore, A. Yariv, Effect of noise on the power spectrum of passively mode-locked lasers, J. Opt. Soc. Am. B 14 (1997) 167–174.
[7] B. Zhu, I.H. White, K.A. Williams, M.R.T. Tan, R.P. Schneider Jr, S.W. Corzine, S. Y. Wang, Ultralow timing jitter picosecond pulse generation from electrically gain-switched oxidized vertical-cavity surface-emitting lasers, IEEE Photonics Technol. Lett. 9 (1997) 1307–1309.
[8] M. Schell, W. Utz, D. Huhse, J. Kässner, D. Bimberg, Low jitter single-mode pulse generation by a self-seeded, gain-switched fabry-perot semiconductor-laser, Appl. Phys. Lett. 65 (1994) 3045–3047.
[9] M. Jinno, Correlated and uncorrelated timing jitter in gain-switched laser-diodes, IEEE Photonics Technol. Lett. 5 (1993) 1140–1143.
[10] A. Martinez, S. Yamashita, Multi-gigahertz repetition rate passively mode-elocked fiber lasers using carbon nanotubes, Opt. Exp. 19 (2011) 6155–6163.
[11] W. Ng, Y.M. So, R. Stephens, D. Persechini, Characterization of the jitter in a mode-locked Er-fiber laser and its application in photonic sampling for analog-to-digital conversion at 10 Gsample/s, J. Lightwave Technol. 22 (2004) 1953–1961.
[12] E. Yoshida, M. Nakazawa, Measurement of the timing jitter and pulse energy fluctuation of a PLL regeneratively mode-locked fiber laser, IEEE Photonics Technol. Lett. 11 (1999) 548–550.
[13] K.A. Williams, I.H. White, D. Burns, W. Sibbett, Jitter reduction through feedback for picosecond pulsed InGaAsP lasers, IEEE J. Quantum Electron. 32 (1996) 1988–1994.
[14] D.J. Derickson, P.A. Morton, J.E. Bowers, R.L. Thornton, Comparison of timing jitter in external and monolithic cavity mode-locked semiconductor-lasers, Appl. Phys. Lett. 59 (1991) 3372–3374.
[15] G.J. Spühler, L. Krainer, E. Innerhofer, R. Paschotta, K.J. Weingarten, U. Keller, Soliton mode-locked Er:Yb:glass laser, Opt. Lett. 30 (2005) 263–265.
[16] K.K. Gupta, D. Novak, H.F. Liu, Noise characterization of a regeneratively mode-locked fiber ring laser, IEEE J. Quantum Electron. 36 (2000) 70–78.
[17] M.J.W. Rodwell, D.M. Bloom, K.J. Weingarten, Subpicosecond laser timing stabilization, IEEE J. Quantum Electron. 25 (1989) 817–827.
[18] U. Keller, K.D. Li, M.J.W. Rodwell, D.M. Bloom, Noise characterization of femtosecond fiber raman soliton lasers, IEEE J. Quantum Electron. 25 (1989) 280–288.
[19] G. Serafino, P. Ghelfi, P. Pérez-Millán, G.E. Villanueva, J. Palací, J.L. Cruz, A. Bogoni, Phase and amplitude stability of EHF-band radar carriers generated from an active mode-locked laser, J. Lightwave Technol. 29 (2011) 3551–3559.
[20] A. Finch, X. Zhu, P.N. Kean, W. Sibbett, Noise characterization of mode-locked color-center laser sources, IEEE J. Quantum Electron. 26 (1990) 1115–1123.
[21] M.J.R. Heck, E.J. Salumbides, A. Renault, E.A.J.M. Bente, Y.-S. Oei, M.K. Smit, R. van Veldhoven, R. Nötzel, K.S.E. Eikema, W. Ubachs, Analysis of hybrid mode-locking of two-section quantum dot lasers operating at 1.5 μm, Opt. Exp. 17 (2009) 18036.
[22] P.J. Delfyett, L.T. Florez, N. Stoffel, T. Gmitter, N.C. Andreadakis, Y. Silberberg, J. P. Heritage, G.A. Alphonse, High-power ultrafast laser-diodes, IEEE J. Quantum Electron. 28 (1992) 2203–2219.
[23] P.J. Delfyett, High-power ultrafast semiconductor-laser diodes, Ultrafast Pulse Gener. Spectrosc. 1861 (1993) 72–83.
[24] M.R.H. Daza, C.A. Saloma, Jitter dynamics of a gainswitched semiconductor laser under self-feedback and external optical injection, IEEE J. Quantum Electron. 3 (2001) 254–264.
[25] E.H. Bottcher, D. Bimberg, Detection of pulse to pulse timing jitter in periodically gain-switched semiconductor-lasers, Appl. Phys. Lett. 54 (1989) 1971–1973.
[26] N.K. Metzger, W. Lubeigt, D. Burns, M. Griffith, L. Laycock, A.A. Lagatsky, C.T. A. Brown, W. Sibbett, Ultrashort-pulse laser with an intracavity phase shaping element, Opt. Exp. 18 (2010) 8123–8134.
[27] A.A. Lagatsky, E.U. Rafailov, C.G. Leburn, C.T.A. Brown, N. Xiang, O. G. Okhotnikov, W. Sibbett, Highly efficient femtosecond Yb:KYW laser pumped by single narrow-stripe laser diode, IEEE Electron. Lett. 39 (2003) 1108–1110.
[28] R. Paschotta, Noise of mode-locked lasers (Part II): timing jitter and other fluctuations, Appl. Phys. B 79 (2004) 163–173.
[29] H. Tsuchida, Pulse timing stabilization of a mode-locked Cr:LiSAF laser, Opt. Lett. 24 (1999) 1641–1643.
[30] N.K. Metzger, ⟨http://home.eps.hw.ac.uk/∼km359/commercial.html⟩ (August 2014).
[31] L.A. Jiang, A. Leaf, M.E. Grein, H. Haus, E.P. Ippen, Noise of mode-locked semiconductor lasers, IEEE J. Sel. Top. Quantum Electron. 7 (2001) 159–167.
[32] A.J. Benedick, J.G. Fujimoto, F.X. Kärtner, Optical flywheels with attosecond jitter, Nat. Photonics 6 (2012) 97–100.
[33] T.K. Kim, Y. Song, K. Jung, C. Kim, H. Kim, C.H. Nam, J. Kim, Sub-100-as timing jitter optical pulse trains from mode-locked Er-fiber lasers, Opt. Lett. 36 (2011) 4443–4445.